Ground state of two-dimensional Yukawa bosons: Applications to vortex melting

W. R. Magro and D. M. Ceperley
National Center for Supercomputing Applications and Department of Physics, University of Illinois, Urbana, Illinois 61801
(Received 23 September 1992; revised manuscript received 9 February 1993)

Using variational and diffusion Monte Carlo techniques, we investigate the ground state of bosons interacting in the continuum through a repulsive modified-Bessel-function potential, $\epsilon K_0(r/\sigma)$, in two dimensions. This is a simplified model for flux lines in high-T_c superconductors. A pair-product trial function is first optimized so that its variational energy is very near the ground-state energy, then the diffusion Monte Carlo technique is used to calculate the exact ground-state energy. As a function of mass and density, we calculate the region of stability of the solid for densities greater than $0.01/\sigma^2$. The quantum crystal melts at high density, due to the potential's soft core, and at low density, due to the exponentially weak interaction. Bosons with $\hbar^2/2m\sigma^2\epsilon > 0.09$ do not crystallize at any density. Within the flux model, we compute the flux-line phase diagram for $Bi_2Sr_2CaCu_2O_8$. Pair-correlation functions, structure factors, and Lindemann ratios at melting are also computed.

I. INTRODUCTION

Bosonic systems are readily studied with current quantum Monte Carlo techniques. The $1/r$, Lennard-Jones, and hard-core potentials have each been studied, both in two and three dimensions.[1–3] Ceperley *et al.* have treated bosons interacting through the three-dimensional Yukawa potential, $V = \epsilon\sigma \exp(-r/\sigma)/r$, determining the liquid-solid phase boundary.[4,5] Bosons interacting with the two-dimensional (2D) Yukawa potential, however, have not yet been treated with exact Monte Carlo methods. In two dimensions, the Yukawa, or screened Coulomb, potential is a modified Bessel function, $K_0(r/\sigma)$, with σ a screening length. This system is of particular interest for its application to high-T_c materials: Nelson *et al.* have proposed a model for flux lattice melting in strongly type-II materials, in which the flux lines are mapped onto a 2D system of bosons interacting via $K_0(r)$.[6]

Xing *et al.* studied the 2D Yukawa system using quantum Monte Carlo techniques.[7] Because they sought to locate the flux liquid regime near H_{c1} they considered densities much lower than those in this paper. Using a pair-product trial wave function plus Gaussian localization for the solid, they first determined its pair-correlation function, $g(r)$, then calculated the variational energy at several densities by scaling $g(r)$. The differing quality of liquid and solid trial wave functions employed, however, leads to a strong variational bias in their estimate of the melting line.

The Yukawa potential has the interesting combination of short range with a soft core. For small r, $K_0(r)$ diverges like $-\ln(r)$; for large r, it decays as $e^{-r}/r^{1/2}$. As in helium, the potential decays rapidly, and the system is liquid at low densities. There is no liquid-gas transition because the potential is purely repulsive. At very high densities, the system approaches a 2D Coulomb system [i.e., a $-\ln(r)$ potential]. Our results may therefore be used to predict the properties of the 2D Coulomb system, in particular its melting density. At moderate densities, and for sufficiently massive bosons, the repulsive potential dominates, and the system crystallizes. We locate this region and compute the threshold mass for crystallization. Because we aim to accurately determine the ground-state properties of the 2D Yukawa system, particularly the melting density, we employ exact as well as variational methods.

Computationally, the Yukawa potential is convenient. At sufficiently low densities, the short range allows the potential to be smoothed to zero at the box edge, making the Ewald method of summing over the periodically repeated particle images unnecessary. In the Coulomb limit a scaling law applies, so that a single transition point determines the high density melting line.

The system considered in this paper consists of N bosons interacting via $\epsilon K_0(r/\sigma)$ in a periodically repeated two-dimensional box with an aspect ratio chosen to perfectly accommodate a triangular lattice. We work in reduced units: lengths are given in units of σ, and energies in units of ϵ, so the Hamiltonian is

$$H = -\sum_i \Lambda^{*2}\nabla_i^2 + \sum_{i<j} K_0(r_{ij}), \tag{1}$$

where i, j are particle indices, and the DeBoer parameter, Λ^*, is defined by

$$\Lambda^{*2} \equiv \frac{\hbar^2}{2m\sigma^2\epsilon}. \tag{2}$$

The reduced density, $\rho = N/A\sigma^2$, and Λ^* are the two dimensionless parameters which characterize the system.

In this paper, we first review the variational and diffusion Monte Carlo methods employed in computing the ground-state properties. We then consider the Jastrow pair term used to form the liquid and solid trial wave functions. Next, we report the results of the computa-

tion: ground-state energies; the (ρ, Λ^*) phase diagram; pair-correlation and structure factors; and Lindemann's ratio at melting. Finally, within the flux model, we study melting in the $Bi_2Sr_2CaCu_2O_8$ compound and compare the resulting phase diagram to other available results.

II. MONTE CARLO TECHNIQUE

Variational Monte Carlo[2] (VMC) is a method used to compute the energy of a many-body trial function, $\psi_T(R)$. We begin by sampling configurations $R = \{\mathbf{r}_1, \ldots, \mathbf{r}_N\}$ from $|\psi_T(R)|^2$ using a Metropolis random walk,[8] where $\mathbf{r}_i$ is the two-dimensional position of the ith of N particles. The variational energy, $E_V \equiv \langle\psi_T|H|\psi_T\rangle$, is then computed as the average of the local energy, $E_L \equiv H\psi_T/\psi_T$, and is an upper bound on the ground-state energy. Our trial function is of the Jastrow pair-product form,[9]

$$\psi_T(R) = \prod_{i<j} \exp[-u(r_{ij})] \prod_i \exp[-c(\mathbf{r}_i - \mathbf{Z}_i)^2], \tag{3}$$

where the $\mathbf{Z}_i$ are lattice sites, r_{ij} is an interparticle distance, and u is the Jastrow pair function. We assume the solid lattice is triangular since that minimizes the potential energy.[10] For the solid, c is an adjustable variational parameter which binds each particle to a lattice site. This method of forming the solid breaks the bosonic symmetry of the particles, but has nonetheless been found to give a good estimate of ground-state properties because exchange energies are small in a crystal.[5] The liquid phase has $c = 0$, and the identical particles are free to traverse the simulation cell. The Jastrow function contains parameters which, along with c, are varied to minimize E_V.[11]

Once a good variational function is found, the exact ground-state energy is computed using diffusion Monte Carlo (DMC).[12] Consider the imaginary time Schrödinger equation,

$$-\frac{\partial\phi(R,t)}{\partial t} = (H - E_T)\phi(R,t). \tag{4}$$

Multiplying this by $\psi_T(R)$ and introducing $f(R,t) = \psi_T(R)\phi(R,t)$, we obtain

$$\frac{\partial f}{\partial t} = \Lambda^{*2}\sum_i \nabla_i^2 f - 2\Lambda^{*2}\sum_i \nabla_i \cdot (f\nabla_i \ln\psi_T) - (E_L - E_T)f. \tag{5}$$

The terms on the right-hand side can be interpreted as diffusion, drift, and branching processes, respectively, of an ensemble of walkers in the $2N$ coordinate space. The initial ensemble, $f(R,0)$, is drawn from the variational Monte Carlo. At large t the distribution of walkers is proportional to $\psi_T(R)\phi_0(R)$, $\phi_0(R)$ being the ground state. The value of E_T that gives a steady population is the ground-state energy. Other properties, such as the pair distribution function, are evaluated in the mixed distribution, $\psi_T(R)\phi_0(R)$. For a sufficiently accurate trial function, we can calculate an observable, $\langle\hat{O}\rangle$, correct to first order in the error of the trial function,[12]

$$\langle\hat{O}\rangle \equiv \langle\phi_0|\hat{O}|\phi_0\rangle = 2\langle\hat{O}\rangle_{\rm DMC} - \langle\hat{O}\rangle_{\rm VMC} + \mathcal{O}\left[(\phi_0 - \psi_T)^2\right]. \tag{6}$$

III. LIQUID AND SOLID TRIAL FUNCTIONS

The form of the Jastrow pair function $u(r)$ is chosen to approximate the solution of the two-body Schrödinger equation. We tried several forms for the pair function and found three which gave good results, each for a certain range of density:[13]

$$u_A(r) = (a + br^2)\cos^2(\pi d\sqrt{w}r)\exp(-wr^2),$$
$$u_B(r) = \frac{a}{1 + wr^2}, \tag{7}$$
$$u_C(r) = a\left(\frac{1}{r+b}\right)^w.$$

Forms A and B for ($\rho = 0.02$, $\Lambda^* = 0.0577$) along with the potential, $K_0(r)$, are shown in Fig. 1. For each calculation w, a, and b were varied to minimize the energy, and d was chosen to be 0.1. For moderate densities, forms A and B gave nearly identical variational energies, though form A was preferred at higher densities. Form C gave the best results at lower densities and is in fact an improved version of that used by Xing *et al.*.[14] In each case the lowest-energy form was used in the subsequent DMC calculation.

IV. RESULTS

The variational method described above has been used to calculate liquid and solid energies at several different values of (ρ, Λ^*). For each density, energies were computed at several values of Λ^* near the liquid-solid transition curve. When the transition was roughly located by comparing variational energies for the liquid and solid, exact DMC calculations were performed at two values of Λ^* chosen to window the transition. The variational parameters, ground-state energies, and other properties for some points near the transition are given in Table I.

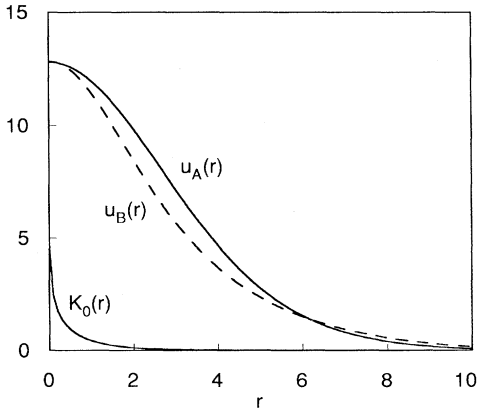

FIG. 1. The optimized Jastrow function, $u_B(r)$, for the liquid at ($\rho = 0.02$, $\Lambda^* = 0.058$). Also shown are the Jastrow function, $u_A(r)$, and the potential, $K_0(r)$.

When determining the melting point, Λ_x^*, variationally, a combination of factors leads to a significant bias. First, the Jastrow wave function better models the solid phase than the liquid, a feature common to many systems. This is apparent from the comparatively large values of $\Delta \equiv (E_{\rm VMC} - E)$ for the liquid shown in Table I. Second, as in the 3D Yukawa system,[5] the energy difference between the phases is very small, even far from the transition. Consequently, the VMC estimate of Λ_x^* is always too large. Figure 2 illustrates the determination of the transition at $\rho = 0.02$. The VMC finds $\Lambda_x^* = 0.081$, while the DMC finds $\Lambda_x^* = 0.052$. This underscores the importance of DMC for locating transitions in this system.

The close-lying energies of the two phases create another difficulty. Even small statistical errors in the computed energies (typically less than 0.1%) can lead to a fairly large uncertainty in Λ_x^*. Consequently, long DMC calculations are required to pin down the transition. For very lengthy DMC calculations, however, the liquid and solid trial functions must give the same result, as there is a unique ground state. Using exact Monte Carlo techniques to locate transitions therefore relies on the metastability of the unfavored phase in the DMC. In the Yukawa system, this metastability is rather fragile, which makes locating the transition and estimating its width difficult.

Although a double tangent construction is difficult, an estimate of the transition width can be made from the pressures, which are computed using the virial theorem and shown in Table I:

$$P = \frac{\rho}{2}[2T + \langle rK_1(r)\rangle]. \tag{8}$$

For small $\delta\rho/\rho$ the relative width of the coexistence region is, to a good approximation,[5]

$$\frac{\delta\rho}{\rho} = |P_{\rm liq} - P_{\rm sol}| \Big/ \left[\rho\left(\frac{dP_{\rm liq}}{\delta\rho}\frac{dP_{\rm sol}}{\delta\rho}\right)^{1/2}\right], \tag{9}$$

where P is the pressure. For $\rho = 0.02$ we find $\delta\rho/\rho = 0.007$, suggesting the transition is very weakly first order. Further studies with path integral Monte Carlo, for example, would be needed to verify this.

We have computed several transition points and obtained the phase diagram shown in Fig. 3. As in the 3D

TABLE I. Results of DMC calculations for liquid and solid (L, S under "Ph") wave functions at points (ρ, Λ^*) near the transition. "Form" indicates the form of the pair function [see Eq. (7)]. w, a, b, and c are the variational parameters in Eqs. (3) and (8). E is the ground-state energy in units of ϵ, with the number in parentheses indicating the standard error in the last digit. T is the kinetic energy, P the pressure. $\Delta \equiv (E_{\rm VMC} - E)$ is a measure of the quality of the trial function.

Λ^*	Ph	Form	w	a	b	c	E/N	T/N	Δ/T	P
						$\rho = 0.4$				
0.1	L	A	0.45	6.2	−0.6	0	$8.472(1)\times10^{-1}$	4.558×10^{-2}	0.18	4.39×10^{-1}
0.1	S	A	0.5	3.4	−0.8	1.1	$8.509(1)\times10^{-1}$	5.295×10^{-2}	0.08	4.42×10^{-1}
0.05	L	A	0.5	13	0.0	0	$7.991(1)\times10^{-1}$	2.548×10^{-2}	0.24	4.26×10^{-1}
0.05	S	A	0.8	7.3	−0.2	1.59	$7.973(2)\times10^{-1}$	2.716×10^{-2}	0.03	4.28×10^{-1}
						$\rho = 0.135$				
0.088	L	A	0.31	7.63	−0.24	0	$1.7239(4)\times10^{-1}$	1.815×10^{-2}	0.13	3.72×10^{-2}
0.088	S	A	0.31	5.39	−0.04	0.56	$1.7255(2)\times10^{-1}$	2.120×10^{-2}	0.03	3.75×10^{-2}
0.069	L	A	0.31	7.87	−0.15	0	$1.6338(4)\times10^{-1}$	1.378×10^{-2}	0.22	3.59×10^{-2}
0.069	S	A	0.31	5.47	−0.18	0.63	$1.6366(2)\times10^{-1}$	1.508×10^{-2}	0.05	3.63×10^{-2}
						$\rho = 0.065$				
0.112	L	A	0.31	5.35	0.95	0	$5.273(6)\times10^{-2}$	1.116×10^{-2}	0.11	6.07×10^{-3}
0.112	S	A	0.45	3.6	0.8	0.39	$5.344(6)\times10^{-2}$	1.404×10^{-2}	0.07	6.19×10^{-3}
0.085	L	A	0.45	5.6	4.0	0	$4.693(1)\times10^{-2}$	9.000×10^{-3}	0.26	5.65×10^{-3}
0.085	S	A	0.45	4.0	2.0	0.39	$4.684(8)\times10^{-2}$	1.020×10^{-2}	0.05	5.75×10^{-3}
						$\rho = 0.03$				
0.075	L	A	0.1	8.0	0.0	0	$9.067(6)\times10^{-3}$	2.895×10^{-3}	0.06	5.58×10^{-4}
0.075	S	A	0.1	6.9	0.0	0.1	$9.104(5)\times10^{-3}$	3.442×10^{-3}	0.04	5.72×10^{-4}
0.065	L	A	0.1	10.2	0.0	0	$8.293(4)\times10^{-3}$	2.716×10^{-3}	0.13	5.27×10^{-4}
0.065	S	A	0.1	8.0	0.0	0.094	$8.236(2)\times10^{-3}$	2.902×10^{-3}	0.04	5.35×10^{-4}
						$\rho = 0.02$				
0.065	L	B	0.11	13.1	—	0	$3.397(3)\times10^{-3}$	1.387×10^{-3}	0.14	1.43×10^{-4}
0.065	S	B	0.11	9.2	—	0.073	$3.411(3)\times10^{-3}$	1.563×10^{-3}	0.05	1.47×10^{-4}
0.058	L	B	0.11	15.0	—	0	$3.085(3)\times10^{-3}$	1.252×10^{-3}	0.16	1.32×10^{-4}
0.058	S	B	0.11	10.6	—	0.074	$3.082(2)\times10^{-3}$	1.368×10^{-3}	0.04	1.35×10^{-4}
						$\rho = 0.01$				
0.032	L	B	0.11	20.7	—	0	$3.582(4)\times10^{-4}$	1.948×10^{-4}	0.14	7.68×10^{-6}
0.032	S	B	0.11	10.4	—	0.06	$3.623(4)\times10^{-4}$	2.149×10^{-4}	0.06	7.93×10^{-6}
0.027	L	C	3.0	1.05	3.1	0	$2.861(4)\times10^{-4}$	1.573×10^{-4}	0.17	6.45×10^{-6}
0.027	S	C	3.0	0.6	2.9	0.051	$2.866(2)\times10^{-4}$	1.622×10^{-4}	0.03	6.61×10^{-6}
0.022	L	C	3.0	1.18	2.9	0	$2.371(7)\times10^{-4}$	1.233×10^{-4}	0.19	5.37×10^{-6}
0.022	S	C	3.0	0.8	2.9	0.048	$2.340(2)\times10^{-4}$	1.294×10^{-4}	0.03	5.66×10^{-6}

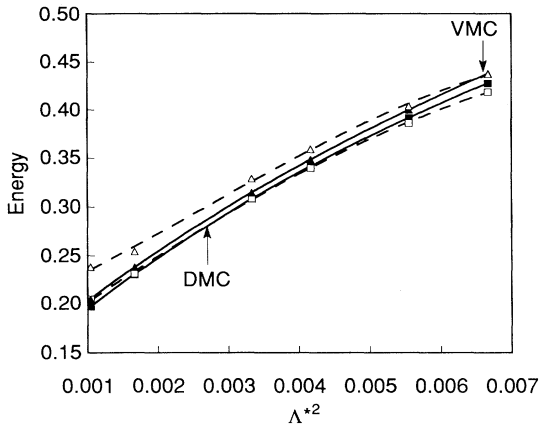

FIG. 2. Variational and exact energies for the solid and liquid at $\rho = 0.02$. The solid lines are a fit to the solid energies. The dashed lines are for the liquid. The lower curves in each pair are the result of DMC. The arrows indicate the VMC and DMC estimates of the transition.

Yukawa system, there is a class of Λ^* for which the kinetic energy dominates, and the system will not crystallize at any density. We estimate this crystallization threshold to be $\Lambda^* = 0.09$. For smaller Λ^*, the liquid is reentrant at zero temperature—the solid will melt on expansion or compression.

Consider now the behavior at high density, where the potential's Coulomb core dominates, and the Hamiltonian effectively becomes

$$\mathcal{H} = -\sum_i \Lambda^{*2}\nabla_i^2 - \sum_{i<j} \ln(r_{ij}). \tag{10}$$

Under the scaling of coordinates $r \to ar$, $\rho \to \rho/a^2$, and $\Lambda^* \to a\Lambda^*$, the Hamiltonian becomes

$$\mathcal{H}' = \mathcal{H} - \frac{N(N-1)}{2}\ln(a). \tag{11}$$

Eliminating a in the scaling relation we find the analytic form of the melting line at high density,

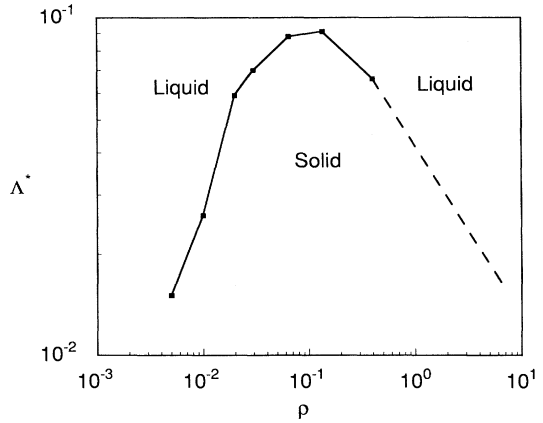

FIG. 3. The phase diagram for Yukawa bosons. Below the line is the solid phase. The squares are transition points computed with DMC. The dashed line at high density is the scaling law, Eq. (12).

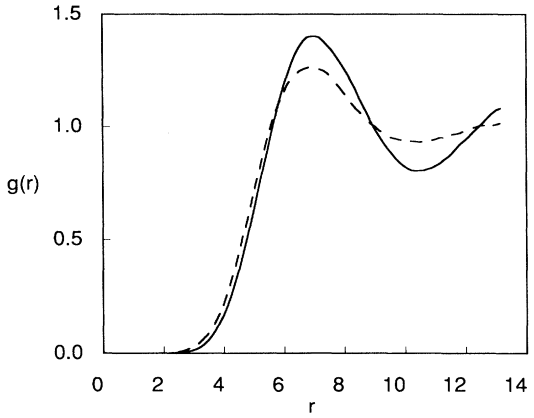

FIG. 4. The variational (- - -) and extrapolated DMC (—) radial distribution function for the liquid far from crystallization at ($\rho = 0.02$, $\Lambda^* = 0.0645$).

$$\lim_{\rho\to\infty} \Lambda_x^* = C\rho^{-\frac{1}{2}}. \tag{12}$$

We use our highest density transition point to estimate the value of the prefactor, $C \approx 0.04$. This high density transition is shown in Fig. 3 as a dashed line.

Figure 4 shows the radial distribution function for the liquid near equilibrium at ($\rho = 0.02$, $\Lambda^* = 0.0645$) computed with variational and diffusion Monte Carlo corrected using Eq. (6). As observed in other quantum liquids, such as the 3D Yukawa system[5] and helium,[15] the ground state has considerably more structure than the liquid trial function provides. Radial distribution functions for the solid near equilibrium at ($\rho = 0.02$, $\Lambda^* = 0.05$) are shown in Fig. 5. As expected, the solid trial function better reproduces the structure of the ground state.

Figure 6 shows structure factors evaluated at the first reciprocal lattice vector from several liquid and solid calculations near melting at $\rho = 0.020$. The kinetic energy increases with Λ^*, forcing the particles to delocalize and the crystal to melt. The system changes very smoothly

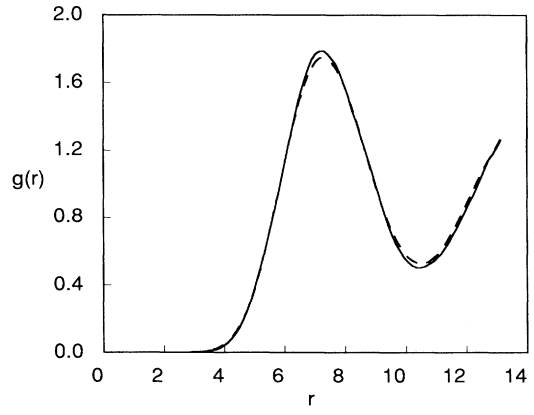

FIG. 5. The variational (- - -) and extrapolated DMC (—) radial distribution function for the solid far from melting at ($\rho = 0.02$, $\Lambda^* = 0.05$).

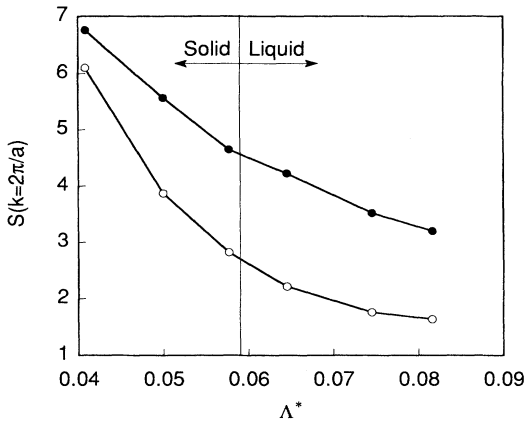

FIG. 6. Extrapolated DMC structure factors for the solid (•) and liquid (○) at $\rho = 0.02$ evaluated at the first reciprocal lattice vector of the triangular lattice, $k = 2\pi/a$, with a the lattice constant. The vertical line indicates the transition.

from liquid to solid, consistent with the narrow coexistence region and the weak metastability of the unfavored phase.

The Lindemann criterion[16] has been useful in describing, but not explaining, melting in classical and quantum systems. It asserts that a crystal will melt when the rms deviation of particles from lattice sites exceeds some fraction of the nearest-neighbor distance. Lindemann ratios (γ) at melting for several densities are given in Table II. Our system typically melted for $\gamma = 0.23$–0.26. While this is lower than typical values in 3D systems, it is consistent with values observed for other 2D systems, including the 2D charged Bose gas and 2D ^{4}He, which melt near $\gamma = 0.254$.[1,3]

V. APPLICATIONS TO FLUX LATTICE MELTING

Nelson *et al.*[6] have shown that the statistical mechanics of the flux-line lattice (FLL) of high-T_c superconductors can be studied through an appropriate mapping onto the 2D Yukawa boson system. In this model, one treats the FLL as a system of 2D bosons with the "Hamiltonian"

$$\mathcal{H} = -\sum_i \frac{(k_B T)^2}{2\tilde{\epsilon}_1}\nabla_i^2 + \sum_{i<j}\frac{\phi_0^2}{8\pi^2\lambda^2}K_0(r_{ij}/\lambda). \quad (13)$$

TABLE II. The "mass," Λ_x^*, and Lindemann ratio, γ, at melting for several densities.

ρ	Λ_x^*	$\gamma_{\rm melt}$
0.01	0.0261	0.23
0.02	0.059	0.26
0.030	0.071	0.26
0.065	0.088	0.24
0.135	0.091	0.26
0.4	0.066	0.26

T is the temperature of the superconductor, $\tilde{\epsilon}_1$ the line tension, ϕ_0 the flux quantum, and λ the London penetration depth in the ab plane. By taking $\sigma = \lambda$ and $\Lambda^{*2} = (2\pi k_B T)^2/\tilde{\epsilon}_1\phi_0^2$ we can interpret our 2D Yukawa results in terms of this model. Each vortex line carries one quantum of flux, so the internal magnetic field is $B = \rho\phi_0\lambda^{-2}$. The other relevant quantities are the external field, H, and the Gibbs free-energy density, g, given by

$$H - H_{c1} = \frac{\phi_0}{2\pi\lambda^2}\left[P/\rho + E\right], \quad (14)$$

$$g = -\frac{\phi_0^2}{8\pi^2\lambda^4}P, \quad (15)$$

where P is the dimensionless 2D pressure computed from Eq. (8). The thermodynamic temperature of the boson system is taken as $\beta_{\rm bose} = \beta_{\rm FLL}L$, with L the thickness of the sample in the c direction. For a sufficiently thick superconducting sample, the corresponding boson system is in its ground state. In the boson ground state the average interparticle spacing is much smaller than the de Broglie wavelength, so the criterion for a "thick" superconductor is

$$L \gg \frac{\tilde{\epsilon}_1(T)\phi_0}{2k_B T B}. \quad (16)$$

The FLL model assumes that the London approach is valid and the field is applied perpendicular to the copper oxide planes. Because the model neglects the angular dependence of the vortex interaction, it applies only when the average vortex tipping angle is small compared to the mass anisotropy, $\left\langle |dr/dz|^2 \right\rangle \ll M_3/M_1$.[17] In the boson system, this condition becomes $T \ll \ln\kappa$, where T is the dimensionless kinetic energy in Table I. This is satisfied in all our calculations.

The general nature of our calculations allows us to apply our results to an arbitrary high-T_c superconductor within the flux-line model. As an example, we choose parameters appropriate for $Bi_2Sr_2CaCu_2O_8$ (BSCCO), where flux lattice melting is especially pronounced. We take $\lambda = 3\times10^{-5}\,{\rm cm}\,(1 - T/T_c)^{-1/2}$,[18] $\kappa = 200$, $T_c = 85\,{\rm K}$, and $M_3/M_1 = 225$. The line tension is $\tilde{\epsilon}_1 = (\phi_o/4\pi\lambda)^2\ln(\kappa)M_1/M_3$. Using relation (14) we compute a phase diagram for BSCCO (Fig. 7). Because the number of flux lines is explicitly conserved, the Helmholtz free energies, rather than the Gibbs free energies, of the two states are equal at the plotted phase boundary.

The DMC simulations of Table I correspond to field strengths $0.1\,{\rm G} < B < 0.5\,{\rm G}$ in BSCCO. The large values of Λ_x^* suggest the FLL would be stable against thermal melting even near T_c at these field strengths. The vanishing line tension near T_c, however, induces Coulomb-like pressure melting. The FLL model breaks down near $H_{c2}(T)$, due to extreme vortex tipping, so the computed flux-line melting field near T_c is not very accurate.

A more interesting case is $H_{c1} \ll H \ll H_{c2}$. Here, the London penetration depth is larger than a typical intervortex spacing, so the logarithmic interaction dominates. Using Eq. (12), the internal melting field in this limit is given by

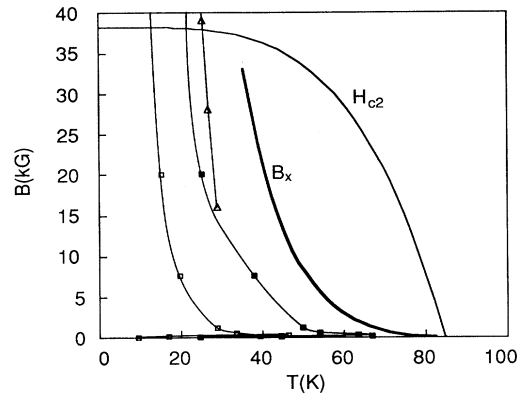

FIG. 7. The phase diagram for $Bi_2Sr_2CaCu_2O_8$, computed within the flux-line model. The high field melting line, $B_x(T)$, is given by Eq. (17). The upper curve is the mean field $H_{c2}(T)$. The open and filled squares are the results of Ryu *et al.* using translational and bond angle order parameters, respectively. The triangles show the measured flux lattice melting in BSCCO by Gammel *et al.* In their sample, $H_{c2}(T=0) = 58\,\mathrm{kOe}$.

$$B_x(T) \approx (0.04)^2 \frac{\phi_0^5}{64\pi^4\lambda^4} \frac{M_1}{M_3} \frac{\ln\kappa}{(k_B T)^2}. \tag{17}$$

At these high field strengths, the boson ground-state pair-correlation function obeys the simple scaling relation, $g_\rho(r) = g_{\rho'}(\sqrt{\rho/\rho'}r)$. We obtain the energies and pressures needed for the corresponding values of H_x with the aid of this relation and the results of a simulation at $\rho = 0.4$. Figure 8 shows the computed magnetic susceptibility at melting, $4\pi\chi_m(H_x) = (B_x - H_x)/H_x$. χ_m vanishes near $H - H_{c1} = 200\,\mathrm{Oe}$, so at high fields B and H may be used interchangeably.

We find that the flux lattice is melted over a significant portion of the phase diagram, well below the mean field value of $H_{c2}(T)$, also plotted in Fig. 7. The shape and position of the melting line in the region $15\,\mathrm{kG} < B < 35\,\mathrm{kG}$ are in rough agreement with measurements of flux lattice melting in BSCCO by Gammel *et al.*[19] They measured $H_{c2}(T=0) \approx 58\,\mathrm{kOe}$, so their melting line extends above our H_{c2}. Their crystals were 0.1 mm thick, easily satisfying criterion (16), so the FLL should be well described by the boson ground state. Precise numerical comparisons are not appropriate, given the varying physical parameters of samples and the steep dependence of $B_x(T)$ on the penetration depth.

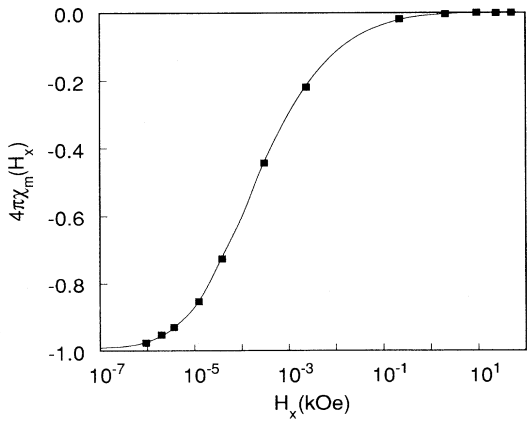

FIG. 8. The computed magnetic susceptibility at melting. The magnetization becomes insignificant above $H_x - H_{c1} \approx 200\,\mathrm{Oe}$, justifying the interchangeable use of H and B at high field strengths.

At sufficiently low fields, the short range of the Yukawa potential prevents the development of long-range order, and the flux lattice melts. Here, the flux interaction is in the exponential limit, and energy differences between solid and liquid are quite small, making the use of an exact method crucial. The convergence of DMC in a reasonable amount of computer time, however, requires good quality trial functions. We have performed variational calculations on the trial wave functions of Xing *et al.* and our modified form of that wave function, u_C of Eq. (7). Although u_C consistently had lower energy than that of Xing, subsequent DMC calculations failed to converge, indicating neither form is adequate at fields much smaller than 0.1 G.

Despite the inherent variational bias and poor convergence, we feel VMC with these wave functions can give order of magnitude estimates of the melting temperature near H_{c1}. While Xing *et al.* found a very narrow liquid regime near H_{c1} in YBCO ($H_x - H_{c1} \approx 10^{-5}$ Oe at 80 K), our results suggest this regime is substantially larger in BSCCO, with $H_x - H_{c1} \approx 10^{-2}$ Oe at 80 K. A better trial wave function is clearly needed to accurately determine the size of the low field flux liquid region.

The phase diagram for BSCCO computed by Ryu *et al.*[20] (shown in Fig. 7) is qualitatively similar to ours, but shows more pronounced FLL melting. In their phase diagram, the crossover from low to high field melting occurs at $B \approx 250\,\mathrm{G}$, while we observe the crossover near $B \approx 1\,\mathrm{G}$. This is expected because the low field region, where energy differences between the phases are smallest, is most sensitive to the "thermal" fluctuations present in thin samples. While our ground-state calculations describe very thick samples, Ryu *et al.* modeled samples with 32 copper oxide planes, or $L \approx 150$ Å. Using the criterion for thick samples above (at $B = 10\,\mathrm{kG}$, $T = 50\,\mathrm{K}$), excited boson states will play a role in FLL melting in samples thinner than several hundred angstroms, disrupting the ground state's positional order and prematurely melting the flux lattice.

VI. CONCLUSIONS

Using exact Monte Carlo methods we have studied systems of bosons interacting at zero temperature with the modified-Bessel-function $K_0(r)$ potential, which is both soft and short ranged. The high density limit of $K_0(r)$ is the 2D Coulomb potential, $-\ln(r)$. This system has been previously studied at low densities by Xing *et al.* using variational Monte Carlo. We have extended the phase diagram to higher densities, and have found that pressure melting sets in for $\rho > 0.1$. Using a scaling argument we have determined the form of the high density

transition line and have estimated its position. From this we predict a melting density parameter $r_s \approx 14$ in the 2D Coulomb bose system.

For light bosons ($\Lambda^* > 0.09$), the kinetic energy dominates, and the system will not crystallize at any density. The energies of the liquid and solid states are very close over a large part of the phase diagram. The relative width of the coexistence region is estimated to be less than 1%. This system is qualitatively quite similar to bosons interacting with the 3D Yukawa potential. The radial distribution function and structure factors indicate that the true ground state has significantly more structure than our liquid trial function provides. We have applied our results to a model BSCCO superconductor and observed flux lattice melting over a large part of the phase diagram. We are currently extending these results to the Coulomb limit, a novel liquid which has no Bose condensate.

ACKNOWLEDGMENTS

One of us (W.M.) was supported by the NSF during the time this research was conducted. We thank D. Nelson for suggesting this calculation and L. Mitas, G. de Lorenzi, and L. Xing for discussions. Most of the calculations were performed on the Cray YMP at the National Center for Supercomputing Applications at the University of Illinois, Urbana. This work was supported by the National Science Foundation under Grant No. NSF-DMR 91-17822.

[1]B. Tanatar and D. M. Ceperley (unpublished).
[2]W. L. McMillan, Phys. Rev. **138**, A442 (1965).
[3]P. A. Whitlock, G. V. Chester, and M. H. Kalos, Phys. Rev. B **38**, 2418 (1988).
[4]D. Ceperley, M. H. Kalos, and G. V. Chester, Phys. Rev. D **13**, 3208 (1976).
[5]D. Ceperley, G. V. Chester, and M. H. Kalos, Phys. Rev. B **17**, 1070 (1978).
[6]D. R. Nelson and S. Seung, Phys. Rev. B **39**, 9153 (1989).
[7]L. Xing and Z. Tešanović, Phys. Rev. Lett. **65**, 794 (1990).
[8]M. Metropolis, A. W. Rosenbluth, H. N. Rosenbluth, A. M. Teller, and E. Teller, J. Chem. Phys. **21**, 1087 (1953).
[9]A. Bijl, Physica **7**, 869 (1940).
[10]A. A. Abrikosov, Zh. Eksp. Teor. Fiz. **32**, 1442 (1957) [Sov. Phys. JETP **5**, 1174 (1957)].
[11]In general the localization parameter, c, was chosen not to exactly minimize the variational energy, but rather to maximize the overlap $\langle \psi_T \mid \phi_0 \rangle$ by ensuring that the Lindemann ratio is the same in the variational and diffusion Monte Carlo.
[12]D. M. Ceperley and M. H. Kalos, in *Monte Carlo Methods in Statistical Physics*, edited by K. Binder (Springer-Verlag, Berlin, 1979).
[13]In practice, u is always smoothed continuously to zero at the box edge.
[14]Xing *et al.* (Ref. 7) chose $b = 0$, so that $u(r \to 0)$ diverges. Their variational energy, however, still has finite variance. By introducing a nonzero b, one can eliminate the divergence and lower the variational energy.
[15]M. H. Kalos, D. Levesque, and L. Verlet, Phys. Rev. A **9**, 2178 (1974).
[16]F. A. Lindemann, Z. Phys. **11**, 609 (1910).
[17]D. R. Nelson (private communication).
[18]Sreeparna Mitra, J. H. Cho, W. C. Lee, D. C. Johnston, and V. G. Kogan, Phys. Rev. B **40**, 2674 (1989).
[19]P. L. Gammel, L. F. Schneemeyer, J. V. Waszczak, and D. J. Bishop, Phys. Rev. Lett. **61**, 1666 (1988).
[20]S. Ryu, S. Doniach, Guy Deutscher, and A. Kapitulnik, Phys. Rev. Lett. **68**, 710 (1992).